ROYAL SOCIETY
OF CHEMISTRY

Check for updates

Preparation and characterization of photopolymerized poly(L-lactide-*co*-ε-caprolactone-*co*-*N*-vinyl-2-pyrrolidone) network as anti-biofouling materials

Shuyin Zuo,[ab] Xiaorong Lan,[b] Yong Wang, [iD][ab] Sai Li,*[a] Zhonglan Tang [iD]*[bc] and Yunbing Wang [iD][b]

The anti-biofouling properties have important applications in the medical field. In this study, cross-linked networks were prepared by photopolymerizing two synthetic macromonomers, including fumaric acid monoethyl ester (FAME) functionalized, three-armed poly(L-lactide) prepolymers (3-PLLA-F) and poly(ε-caprolactone) prepolymers (2-PCL-F), with *N*-vinyl-2-pyrrolidone (NVP) as the diluent. The prepared networks were characterized by their thermal properties, mechanical properties, cytotoxicity experiments and anti-biofouling properties. The Young's modulus and tensile strength of networks decreased by increasing PCL content. In contrast, the elongation of networks significantly increased. Moreover, no obvious cytotoxicity was observed, and the adhesion of L929 fibroblasts and platelets was resisted. Combined with Digital Light Processing technology (DLP) in the future, the designed polymer network could potentially be commercial in the field of biological anti-fouling materials.

1. Introduction

Anti-biofouling properties play critical roles in many medical applications such as medical implants, biosensors and separation membranes.[1] Research and development of anti-biofouling materials for reducing the side effects of implant materials in the healing process, such as inflammation, thrombosis and blood coagulation, has important value in clinical applications. So far, a variety of biocompatible polymers have been synthesized and developed, including polyvinyl alcohol, poly(*N*-vinyl-2-pyrrolidone), poly(2-oxazoline), polyethylene glycol and zwitterionic polymers.[2]

These polymers possess strong anti-biofouling capability and good biocompatibility. However, most of the molecular chains were polyacrylate or polyacrylamide, which are not biodegradable. These materials could not be metabolized in the body, then remain in the body to form foreign bodies, which would disturb the metabolism of normal cells. One of the future development directions of anti-biofouling materials is to develop biodegradable antifouling materials to expand their research and application in the biomedical field. Biodegradable antifouling materials could be obtained by introducing antifouling functional molecules into biodegradable matrix

molecules (such as aliphatic polyesters, polycarbonates). I. Dueramae *et al.* synthesized a novel polyurethane with high mechanical properties and non-toxic degradation products. Poly(carboxymethyl betaine) was interpenetrated in novel polyurethane materials, to achieve additionally anti-biofouling property. The novel materials would be expected to be used in aneurysm and postoperative adhesion prevention.[3] Guoxiong Dai *et al.* prepared biodegradable copolymer with good anti-fouling efficacy for more than 6 months.[4] The improved anti-fouling efficacy was attributed by the optimal main-chain degradation as well as the side-group hydrolysis.

The current medical products applied in the market are not suitable for personalized medical needs, because most of them were manufactured by the technology of assembly-line production and then put into use. However, for the implant material *in vivo*, personalized product could reduce the additional adverse effects owing to a high-precision size at the implant site and the most matched mechanical properties. Recently, 3D printing technologies have been applied in many biomedical material productions. Among 3D printing technology, Digital Light Processing technology (DLP), which possesses the advantages of higher printing accuracy and faster printing speed rather than Fused Deposition Modeling (FDM), is based on polymerizing liquid photosensitive resin layer by layer. Robert van Lith *et al.* developed a bioresorbable biomaterial ink. Due to the polymerization by exposure to ultraviolet light, this ink could be used for fast 3D printing. With the customizable, compressed and self-expanded properties within

[a]School of Chemical Engineering, Sichuan University, China

[b]National Engineering Research Center for Biomaterials, Sichuan University, China. E-mail: tang.zhonglan@scu.edu.cn; Tel: +86-28-6423-2936

[c]Institute of Regulatory Science for Medical Device, Sichuan University, China

a clinically relevant time frame, this ink could be potential to print a customizable, patient-specific stent for the patients with an arterial blockage.[5] Le Hoang Sinh *et al.* demonstrated a novel photo-curable polyurethane resin for stereolithography, which could accurately and precisely simulate artificial skin blood vessel model.[6]

There are few reports on the application of resins combined with UV-curing 3D molding technology to obtain degradable materials for anti-biofouling. In our previous work, a cross-linked network of functionalized poly(L-lactic) (PLLA) with NVP was developed for application in the field of antifouling.[7] PLLA was confirmed to be non-toxic, low cost in use, good mechanical properties, biocompatible and biodegradable, thus has attracted much attention in the biomedical polymer field.[8–10] Poly(N-vinyl-2-pyrrolidone) (PVP) possesses strong anti-biofouling capability and good biocompatibility, which has been used as a blood plasma substitute.[11–13] However, PLA is generally considered to be a brittle polymer.[14] When copolymerization with poly(ε-caprolactone) (PCL), which exhibits high flexibility and low glass transition temperature, the toughness of PLA could increase.[15,16] At present, poly(ε-caprolactone) derivatives prepared by introducing antifouling molecules, as antifouling materials, have been described in some literatures.[17,18]

In this study, to increase the toughness of the network, PCL chains was introduced in PLLA/NVP cross-linked networks. 2-PCL was end-functionalized with fumaric acid monoethyl ester (FAME). Since fumaric acid is a compound naturally found in the body, fumaric acid derivatives are attractive compounds for end-functionalization reactions without toxicity upon implantation.[19] The photosensitive resin has achieved by mixing photosensitive FAME-functionalized 3-PLLA prepolymers with photosensitive FAME-functionalized 2-PCL prepolymers, reactive diluent of NVP and photoinitiator of Irgacure 2959. A complex PLLA/PCL/NVP cross-linked network was formed by UV curing. Therefore, a poly(L-lactide) material modified by poly(ε-caprolactone) was prepared, and its thermal properties, hydrophilicity, mechanical properties, biocompatibility and antifouling properties were studied.

2. Materials and methods

2.1. Materials

L-Lactide was obtained from Jinan Daigang Biomaterial Co., Ltd. (Shandong, China), which was purified by recrystallization from anhydrous ethyl acetate twice before used. Poly(ε-caprolactone) diol (2-PCL) with a nominal number-average molecular weight (M_n) of 2000 g mol^{-1} and Tin 2-ethylhexanoate (Sn(Oct)$_2$) were purchased from Sigma Aldrich (Darmstadt, Germany). NVP was obtained from Chengdu Best Reagent Co., Ltd. (Chengdu, China). 4-Dimethylaminopyridine (DMAP), fumaric acid monoethyl ester (FAME), 1,3-dicyclohexylcar-bodiimide (DCC) and Irgacure 2959 (2-hydroxy-1-[4-(hydroxyethoxy) phenyl]-2-methyl-1-propanone) were purchased from Tokyo Chemical Industry (Tokyo, Japan). Toluene (b.p. 111 °C) and dichloromethane (b.p. 40 °C) were obtained from Chengdu Kelong Chemical Reagent Factory (Chengdu, China), and distilled from calcium hydride before used.

Dulbecco's modified eagle medium (DMEM), phosphate buffer solution (PBS), fetal bovine serum (FBS), and penicillin–streptomycin mixture were purchased from Thermo Fisher Scientific Co., Ltd (Waltham, MA). 4′,6-Diamidino-2-phenylindole (DAPI) and tetramethylrhodamine–phalloidin (TRITC–phalloidin) were received from Solarbio Life Sciences Co., Ltd (Beijing, China). Water used in this study was purified by a water purification system (PCDX-WJ) (Pincheng Science and Technology Ltd., Sichuan, China) unless otherwise mentioned.

All animal procedures were performed in accordance with the animal use regulations of the Animal Protection Commission of China and Sichuan University, and experiments were approved by the Medical Ethics Committee of Sichuan University (SN: K2019014).

2.2. Preparation of three-armed PLLA prepolymers

Three-armed poly(L-lactiede) prepolymer (3-PLLA) was prepared according to a previous reported.[7] Briefly, 3-PLLA was synthesized by using glycerol as an initiator to ring-open and polymerize L-lactide (LLA) (Fig. 1A). Glycerol, LLA, and Sn(Oct)$_2$ as a catalyst were dissolved in dry toluene, which was performed degassing by three freeze–pump–thaw cycles. Under argon protection, the radical polymerization was conducted at 80 °C. After 24 h, the reaction mixture was then poured into an excess amount of diethyl ether to precipitate 3-PLLA. The precipitated compound was obtained through a filter and dried under vacuum.

2.3. Preparation of FAME-functionalized 3-PLLA and 2-PCL prepolymers

FAME-functionalized 3-PLLA (3-PLLA-F) and 2-PCL (2-PCL-F) prepolymers were prepared *via* esterification reaction between hydroxyl groups at the terminal of oligomer chains and carboxyl group of FAME, respectively (Fig. 1B and C). The 2-PCL or 3-PLLA were dissolved in dry DCM with a three-necked round-bottom flask, which was connected with two-way stopcocks and a drooping funnel. The reaction mixture was stirred at 0 °C for 30 min under argon atmosphere. Then, an exceeded amount of FAME was added into the mixture. After complete dissolution, a DCM solution containing DCC as a coupling agent and DMAP as a catalyst was added dropwise to the former stirred solution at 0 °C. After being stirring under argon protection for 48 h, the solution was filtered to remove dicyclohexylurea and subsequently purified by precipitation in cool ether, filtration and vacuum drying.

2.4. Resin formulation and network preparation

3-PLLA-F and 2-PCL-F were diluted with NVP (50 wt%) in different weight ratios. Irgacure 2959 (5% of total mass) was added to the resin as a photoinitiator. After 30 min vacuum degassing, the resultant resin was carefully spread on a Teflon® mould. A cross-linked network was formed (Fig. 1D) by irradiating specimens cast with 365 nm UV light (INTELLIRAY 600, intensity 50 mW cm^{-2}) for 180 seconds. After exposing, the samples were extracted with alcohol three times for 10 minutes
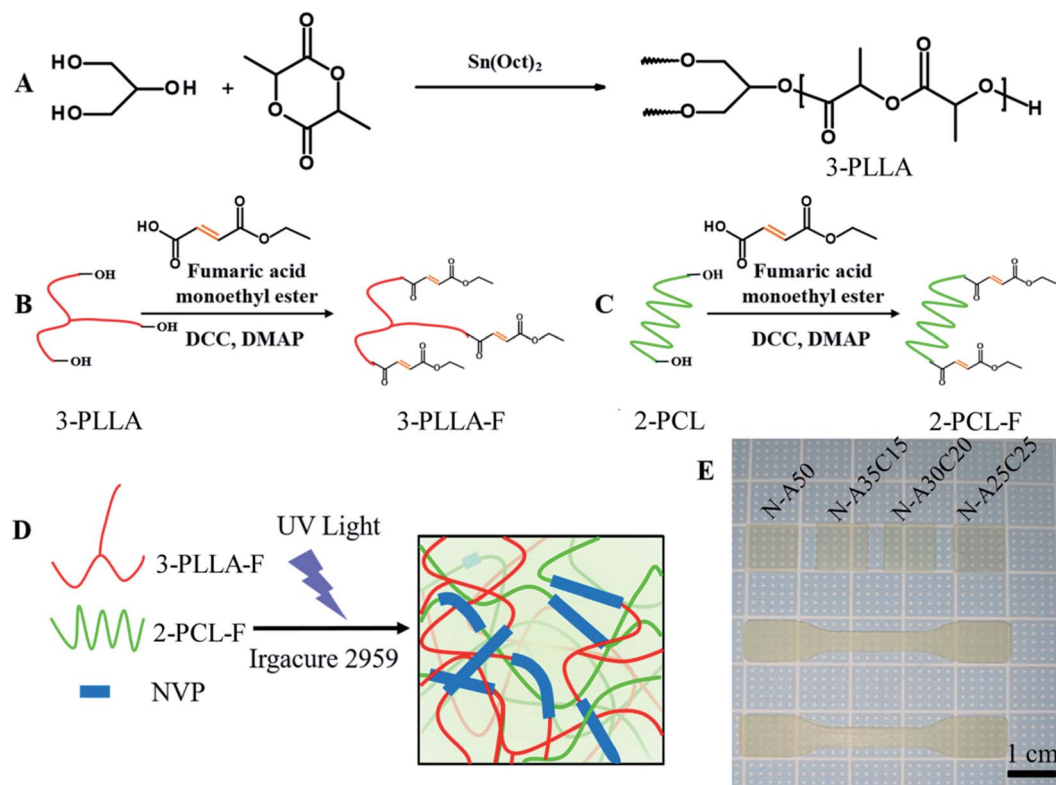
Fig. 1 Synthetic schemes of 3-PLLA (A), FAME-functionalized 3-PLLA prepolymer (3-PLLA-F) (B) and FAME-functionalized 2-PCL prepolymer (2-PCL-F) (C). A schematic to describe the formation of cross-linked networks (D). 3-PLLA-F, 2-PCL-F and NVP polymers are covalently cross-linked upon exposure to UV light in the presence of Irgacure 2959 photoinitiator to form a highly elastic network. The specimen sheets (10 × 10 × 0.5 mm) and the dumbbell-shaped test specimen (50 × 10 × 1 mm) from prepared resins were obtained (E).

each to strip soluble impurities and dried at 60 °C overnight. In this study, the dumbbell-shaped test specimen (50 × 10 × 1 mm) and the specimen sheets (10 × 10 × 0.5 mm) were prepared. Throughout this paper, all networks are labelled as N-AXCY, in which X stands for the content of 3-PLLA-F of networks and Y for 2-PCL-F. For example, N-A25C25 stands for the network obtained after photo-polymerisation of PLLA-F (25 wt%), PCLD-F (25 wt%) and NVP (50 wt%).

2.5. Chemical characterization of prepolymers

The M_n of 3-PLLA and 3-PLLA-F, and their polydispersity (M_w/M_n) were measured by a gel permeation chromatography system (GPC, Agilent 1260 Infinity). The powder of 3-PLLA and 3-PLLA-F were dissolved in chloroform solution. The calibration curve was prepared with a series of monodisperse polystyrene standards, while the chloroform (HPLC grade) was used as the eluent. The GPC analysis was performed with 30 μL polymer solution at a flow rate of 1 ml min^{-1} at 35 °C.

Proton nuclear magnetic resonance (^{1}H NMR) spectra of 3-PLLA, 3-PLLA-F, 2-PCL and 2-PCL-F were monitored by an AV III HD 400 MHz NMR spectrometer (Bruker, Germany). All samples were dissolved in deuterated chloroform. The degrees of functionalization of products were measured from the spectra. A total of 32 scans were acquired for each ^{1}H NMR spectra. Chemical shifts (δ) were given in ppm with respect to

tetramethylsilane. Unless otherwise indicated, all were run at room temperature (24 ± 1 °C).

To assess further whether FAME was integrated in both ends of the polymer chain, Fourier Transform Infrared Spectrometer (FTIR spectrometer) with attenuated total reflection mode was used on 3-PLLA, 3-PLLA-F, 2-PCL and 2-PCL-F. Each sample of polymer power mixing with 10 mg of KBr was compressed to prepare pellet. The pellets were placed into the holder of FTIR spectrometer (INVENIO R Bruker, Germany), and 16 scans with a resolution of 4 cm^{-1} were performed. The data was analyzed using OriginPro 8 software.

2.6. Thermal characterization of prepolymer

Differential scanning calorimetry (DSC) was performed to study the thermal properties of the prepared networks with the TGA/DSC 3 + (Mettler Toledo, Switzerland) in a nitrogen atmosphere. In order to eliminate the thermal history, all of samples (10–15 mg) were heated from 30 to 180 °C at a heating rate of 10 °C min^{-1}, and then kept isothermal for 5 min, cooled to 30 °C at 10 °C min^{-1}. After 5 min, a second heating scan was recorded under nitrogen gas flow rate of 50 ml min^{-1}.

2.7. Characterization of polymer networks

2.7.1. Water contact angle measurement. Water contact angle of resultant networks were determined by using a contact

angle measurement system with a digital camera and image analysis software (Attension Theta, Biolin Scientific, Finland). In order to keep samples flat during the drying process, these specimens ($10 \times 10 \times 1$ mm^3) were placed between two glass slides. Water drops with 5 μL generated by a micrometric syringe was deposited on the specimen sheets, and the contact angle value was monitored within the following 30 s. The collected information was analyzed using the OneAttension software. Eight independent measurements with different sites of the sample were averaged.

2.7.2. Tensile testing. Tensile tests of dumbbell-shaped test specimens were carried out at room temperature using a universal tensile machine (INSTRON 3366 USA) equipped with a 1000 N load cell at 5 mm per minute speed. Young's modulus, tensile strength, elongation and fracture energy were measured from stress–strain curves. Five samples were tested for each of polymer networks to obtain the average values and standard deviations.

2.7.3. *In vitro* degradation. The specimen sheets were used to study the degradation of polymer network *in vitro*. After weighing, the various specimens were incubated in a tube containing 10 ml of PBS solution (pH 7.4) at 37 °C to obtain relative degradation data among samples. The PBS solution was refreshed every 4 weeks during the entire process. Then, samples were collected from the PBS at time points, washed with purified water, freeze-dried for 1 week and weighed. Mass loss percentages were calculated using the following equation, where the W_0 is the initial mass, W is the mass measured at a given time point. The results are presented as the average $\pm$ standard deviation of at least 5 individual measurements

$$\text{Mass loss (\%)} = (W_0 - W)/W_0 \times 100$$

2.7.4. Cell cytotoxicity and morphology. To evaluate the biocompatibility of polymer networks, the effect of samples' leaching liquor on the growth of L929 mouse fibroblast cells (MFCs) was studied, according to guidelines stated by ISO 10993-12:2012. The front and back of each specimen sheet was sterilized by UV exposure for 30 min, respectively. Then each sample was immersed in a tube containing 4 ml serum-free medium (1% penicillin–streptomycin) for 24 h or 72 h at 37 °C. The extract of each sample was added 10% v/v FBS for cell culture.

MFCs were seeded by adding 100 μL cell suspension in 96-well plates (3000 cells per well) and cultured for 6 h. After MFCs were confirmed to adhere on the surface of well, the culture medium was replaced by the sample extract with FBS. MFCs were continued to culture for 1 d, 3 d and 5 d. MFCs on the plate were counted at each time point by using the Cell Counting Kit-8 (CCK-8) assay. To study the morphology of MFCs under the sample extract, MFCs were cultured in 24-well plates with a similar procedure. Namely, MFCs were seeded in 24-well plates with same cell density, and cultured for 6 h. Then the sample extract with FBS was used to culture the cells instead of original medium. Cell morphology was monitored by using an inverted light microscope. High molecular weight polylactide

(HW-PLA) sheets and tissue culture polystyrene (TCPS) were used as a control sample.

2.7.5. Cell seeding on polymer networks. The specimen sheets were placed in the middle of the wells in 24-well plates. A stainless-steel ring was put on the top of the sample to prevent the sheet from floating. MFCs were seeded on the surface of specimens directly at a density of 30 000 cells per well and incubated for 24 h and 72 h in a cell incubator, respectively. After this time period, cells were fixed by formalin (4% para-formaldehyde) and permeabilized using 0.5% Tiriton X-100. The specimens were stained using DAPI and TRITC–phalloi-din. Fluorescent images were recorded by using a confocal laser scanning microscope (CLSM) (Nikon A1R MP+). Then, the specimens were observed by SEM (JEOL, JSM-7500F, Japan) followed by fixation, dehydration, freeze-drying treatment and gold spray treatment.

2.7.6. Platelet adhesion. To preserve platelet activity, the blood sample was collected from rabbit by using blood collection tubes containing sodium citrate. The tubes were centrifuged at 1000 rpm for 15 min to obtain platelet-rich plasma (PRP) supernatant. The specimen sheets were cut into disk-shape using a cork borer, to fit the size of 96-well plate. Disk-shaped specimens were plated into 96-well plates, and then immersed in 100 μL platelet-rich plasma (PRP) at 37 °C for 1 h. After PRP was removed from each well, the sheets were washed with PBS three times. The morphology of adherent platelets on sheets was observed by SEM followed by fixation, dehydration, freeze-drying treatment and gold spray treatment.

2.7.7. Bacterial adhesion. To further study anti-bacterial adhesion of resultant networks, *E. coli* was selected to evaluate bacterial adhesion. Quantification of bacterial adhesion on resultant networks was carried out by the spread plate method. The sterilized specimens were placed in 48-well microplates with 300 μL *Escherichia coli* suspension (*E. coli*, $\sim 2 \times 10^7$ ml^{-1}), and incubated at 37 °C for 4 hours at a constant temperature. Then *E. coli* solution was sucked out of the hole and gently cleaned 3 times with 500 μL PBS. Subsequently, incubated specimens were put in centrifuge tubes containing 500 μL PBS, sonicated for 7 min to detached adhering bacteria. Finally, 100 μL of bacterial suspension diluted 100 times were put onto the Luria broth (LB) agar plate. Incubate for one day at 37 °C and calculate colony-forming units (CFUs) on LB agar plates.

3. Results and discussion

3.1. Preparation of 3-PLLA

3-PLLA was prepared by ring-opening polymerization of L-lactide with glycerol as a trifunctional initiator. The chemical structure of the synthesized polymer was characterized by ^{1}H-NMR. As shown in Fig. 2A, two sharp proton peaks at $\delta = 5.16$ ppm and $\delta = 1.58$ ppm belonged to the methylene (3) and methyl (4) of the L-lactide repeat unit, respectively. The weak peak at $\delta = 4.37$ ppm was attributed to the terminal hydroxyl group of 3-PLLA (5′). These results indicated that PLLA oligomers were successfully synthesized. The degree of polymerization of 3-PLLA in each arm has been calculated as 7.65 by ^{1}H-NMR according to the previous reported method.[7] As a result,
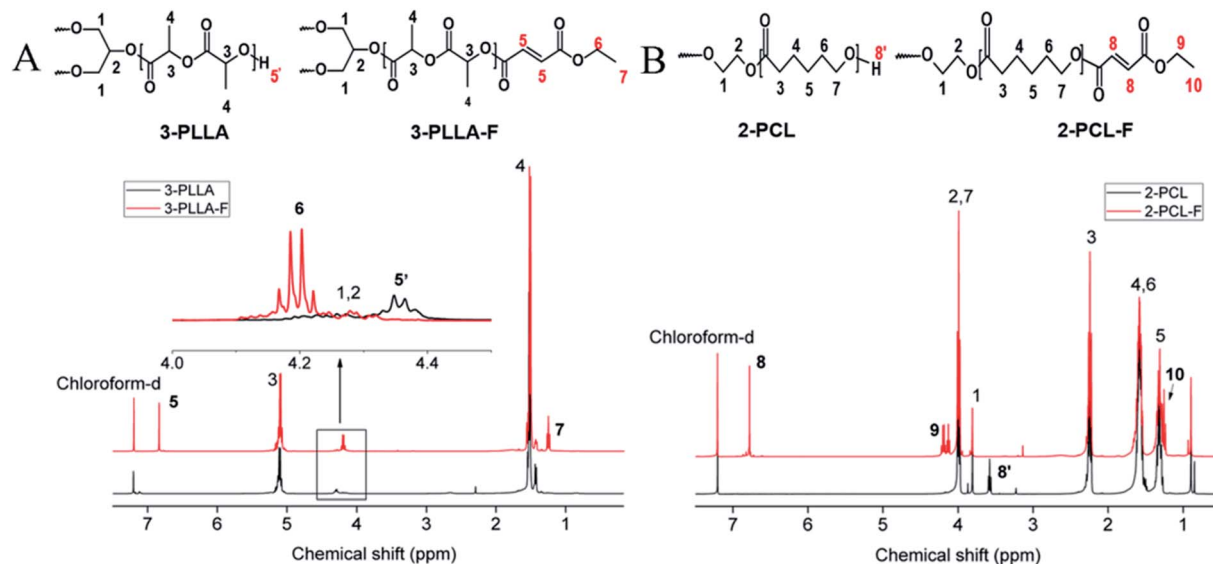
Fig. 2 ^{1}H NMR spectra dissolved in chloroform-*d*. (A) The spectra of 3-PLLA and 3-PLLA-F. (B) The spectra of 2-PCL and 2-PCL-F.

the M_w of 3-PLLA was about 3400 g mol^{-1}. By a GPC system the M_n and polydispersity of 3-PLLA were determined as 4500 g mol^{-1} and 1.17, respectively. Such narrow molecular weight distribution has also been reported in other literatures,[20–22] which has been explained that alcohol-induced ring-opening polymerization of lactones could yield star copolymers.

3.2. Preparation and characterization of prepolymer

The prepolymers of 3-PLLA-F and 2-PCL-F were prepared by coupling of 3-PLLA and 2-PCL with FAME. The ^{1}H NMR spectra were measured to confirm the esterification reaction. As shown in Fig. 2A, the proton peak of hydroxyl (5′, $\delta = 4.37$ ppm) belonged to 3-PLLA disappeared, and the proton peaks of double bond (5, $\delta = 6.83$ ppm) and ethyl group (–CH$_2$–, 6, $\delta = 4.25$ ppm; –CH$_3$, 7, $\delta = 1.32$ ppm) appeared. Similarly, as shown in Fig. 2B, the proton peak of hydroxyl (8′, $\delta = 3.58$ ppm) belonged to 2-PCL disappeared, and the proton peaks of double bond hydrogen (8, $\delta = 6.83$ ppm) and ethyl group (–CH$_2$–, 9, $\delta =$

4.25 ppm; –CH$_3$, 10, $\delta = 1.32$ ppm) appeared. These results indicated that active double bond has been introduced at the end of polymer chain resulting in the photosensitivity prepolymer of 3-PLLA-F and 2-PCL-F. The degrees of substitution assigned to the ratio of fumarate groups substituted for hydroxyl groups was calculated to be about 97% and 91% for 3-PLLA-F and 2-PCL-F, respectively, based on the integral of the peak intensity of double bond at $\delta = 6.83$ from the NMR spectrum. The high degree of substitution indicated the high functionalization of double bond, which could provide enough photosensitive sites in the following polymerization.

To further confirm the functionalization of 3-PLLA and 2-PCL, the chemical structures of 3-PLLA-F and 2-PCL-F were characterized by FTIR spectroscopy. FTIR analysis of resultant 3-PLLA-F showed the presence of small peak at 1645 cm^{-1}, which stands for the characteristic peak of –CH=CH– bonds of 3-PLLA-F (Fig. 3A). 3-PLLA and 3-PLLA-F had a strong peak around 1745 cm^{-1} due to –C=O moieties. FTIR spectrum for 3-
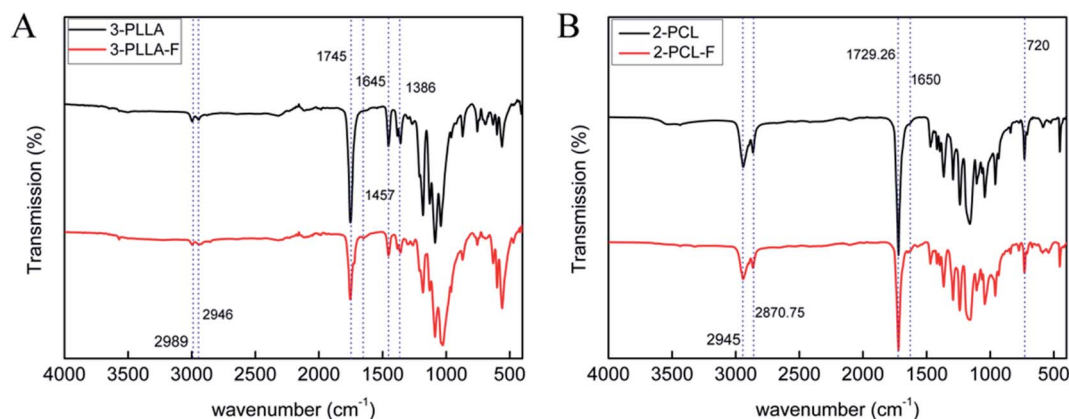

Fig. 3 FTIR spectra. (A) The spectra of 3-PLLA and 3-PLLA-F. (B) The spectra of 2-PCL and 2-PCL-F.

PLLA and 3-PLLA-F exhibited characteristic peaks at 2989 cm^{-1} (–CH$_2$–, asymmetric and stretching) and 2946 cm^{-1} (–CH$_2$–, symmetric stretching). These absorption peaks indicated that FAME was successfully introduced into 3-PLLA, which is consistent with the results of NMR.

Similarly, FTIR spectrum of 2-PCL and 2-PCL-F was shown in Fig. 3B. FTIR spectrum of the 2-PCL-F exhibited characteristic peaks at 1650 cm^{-1} (–CH=CH–, stretching), 2945 cm^{-1} (–CH$_2$–, asymmetric and stretching), 2870 cm^{-1} (–CH$_2$–, symmetric stretching) and 1729 cm^{-1} (–C=O, stretching), indicating that 2-PCL-F was successfully synthesized, which is consistent with the results of NMR.

3.3. Preparation and characterization of polymer networks

Photosensitive resin was prepared by mixing 3-PLLA-F, 2-PCL-F, NVP as active solvent and Irgacure 2959 as a biocompatible initiator. Upon irradiation of UV-light, Irgacure 2959 molecules dissociate into radicals, which initiate the addition photo-polymerization of 3-PLLA-F, 2-PCL-F and NVP, resulting in a cross-linked network (Fig. 1D and E). Three kinds of polymer networks were prepared with different ratio of polymers, which were labeled as N-A35C15, N-A30C20, N-A25C25, and N-A50 as control.

3.3.1. Thermal characterization of networks. The glass transition temperatures (T_g) of polymer networks in the dry state were determined by DSC. The T_g of PLLA, PCL and PVP were measured as 54.3 °C, −61.9 °C and over 120 °C in previous studies, respectively.[23–25] As shown in Table 1, each sample was only detected a single glass transition, which was belonged to random copolymers of network. These results indicated that components were homogeneously incorporated into the network structure.

3.3.2. Water contact angle measurement. The wettability of specimens was evaluated by measuring static water-in-air contact angle by the sessile-drip method at room temperature (Fig. 4). The water contact angles (WCA) of N-A35C15, N-A30C20, and N-A25C25 were measured as 89.8°, 88.3°, and 92.2°, respectively, which were slight less as that of N-A50 (95.6°). No tendency was observed, though the 2-PCL-F content in the networks was increased from 15 to 25%. In our previous study, the WCAs of PLLA/NVP cross-linked network
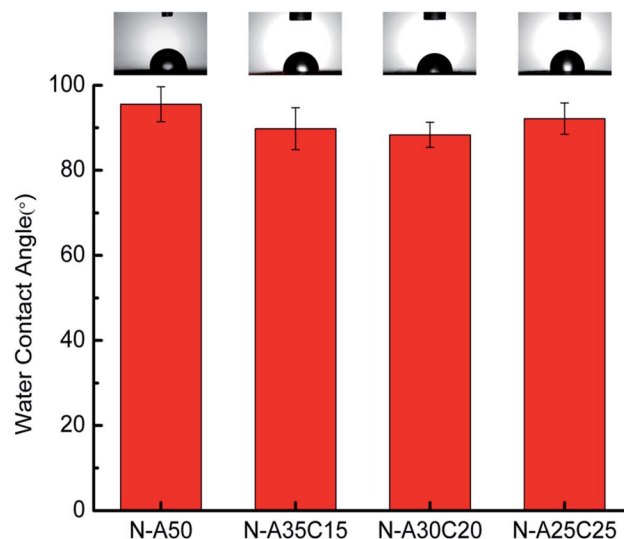
Table 1 Glass transition temperatures of networks prepared with 3-PLLA-F, 2-PCL-F and NVP[a]

	2-PCL-F content (wt%)	T_g (°C)
N-A35C15	15	68.23
N-A30C20	20	68.33
N-A25C25	25	66.98

[a] N-A35C15: the network obtained after photo-polymerisation of PLLA-F (35 wt%), PCLD-F (15 wt%) and NVP (50 wt%). N-A30C20: the network obtained after photo-polymerisation of PLLA-F (30 wt%), PCLD-F (20 wt%) and NVP (50 wt%). N-A25C25: the network obtained after photo-polymerisation of PLLA-F (25 wt%), PCLD-F (25 wt%) and NVP (50 wt%).

Fig. 4 Static water-in-air contact angle measurements for N-A50, N-A35C15, N-A30C20 and N-A25C25.

decreased with hydrophilic segment of NVP content increased. In this study, the replacement of 2-PCL-F content barely changed the wettability of specimens, since PCL is well known as hydrophobic polymer as similar as PLA, and the PVP content was maintained as 50%.[26] Moreover, as mentioned above, compared with 3-PLLA-F, more hydroxyl groups remained in 2-PCL-F, because of the lower substitution of hydroxyl groups confirmed by ^{1}H NMR. The residual hydroxyl groups surface in PLLA/PCL/NVP cross-linked network could increase the hydrophily on the material resulting in a lower WCA.

3.3.3. Tensile testing. The mechanical properties of N-A35C15, N-A30C20, N-A25C25, and N-A50 networks were shown in Fig. 5. PLLA/PCL/NVP polymer networks exhibited ductile fracture during tensile, which were incarnated by yield phenomenon and plastic deformation, elongation increase and fracture energy increase. The resultant PLLA/NVP cross-linked
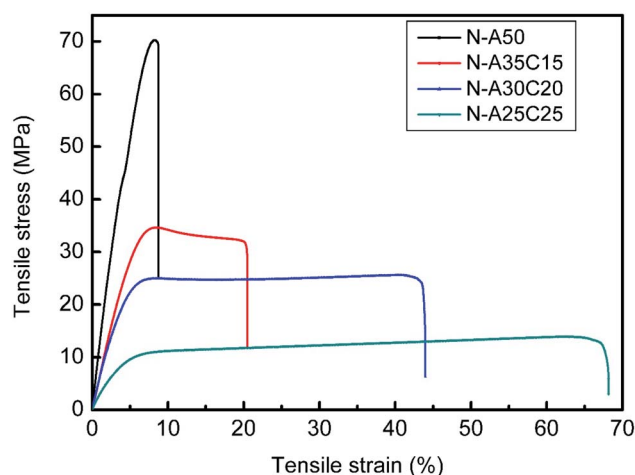

Fig. 5 The stress−strain curve of N-A50, N-A35C15, N-A30C20, and N-A25C25 with a 1000 N load cell.

Table 2 Tensile properties of N-A50, N-A35C15, N-A30C20 and N-A25C25[a]

	Young's modulus (Mpa)	Tensile strength (Mpa)	Elongation (%)	Fracture energy (MJ m^{-3})
N-A50	1238 ± 22	71.8 ± 3.2	8.8 ± 1.0	373 ± 8
N-A35C15	749 ± 93***	37.0 ± 3.9****	19.6 ± 4.4***	579 ± 9****
N-A30C20	601 ± 6****	25.5 ± 0.8****	39.2 ± 6.7***	1194 ± 12****
N-A25C25	94 ± 1****	13.9 ± 0.1****	65.4 ± 3.9****	738 ± 1****

[a] The data in the table were expressed as mean ± standard deviation; $*p < 0.05$, $**p < 0.01$, $***p < 0.001$, $****p < 0.0001$.

network of N-A50 was brittle fracture with a very low elongation of 8.8%. When 15% of 2-PCL-F was mixed, PLLA/PCL/NVP cross-linked network was observed exhibited neck propagation after yielding, and the elongation increased dramatically to 19.6%. The tensile toughness was obviously improved. The elongation of N-A30C20 and N-A25C25 samples increased to 39.2% and 65.4%, respectively. The carbon chain structure of 2-PCL-F possesses good flexibility and machinability, so it can increase tensile toughness of PLLA/PCL/NVP networks. However, young's modulus and tensile strength decreased as 2-PCL-F content increased. The young's modulus and tensile strength of N-A35C15 was decreased to 749 ± 93 and 37 ± 3.9 MPa, respectively, which were significantly lower than those of N-A50 (1238 ± 22 and 71.8 ± 3.2 MPa). Similarly, all of these for N-A30C20 (601 ± 6 and 25.5 ± 0.8 MPa) and N-A25C25 (94 ± 1 and 13.9 ± 0.8 MPa) crosslinked networks were further reduced. It remains a striking fact that toughness is achieved by sacrificing strength and modulus. The fracture energy of resultant networks was calculated by the integral area under the stress–strain curve. As shown in Table 2, compared with the fracture energy of N-A50 resultant networks for 373 MJ m^{-3}, the fracture energy of resultant networks contained 2-PCl-F was increased, thus the tensile fracture toughness was improved. Among our three resultant networks, N-A30C20 possesses the largest fracture energy of 1194 MJ m^{-3}. As for N-A35C15 and N-A30C20

resultant networks, the fracture energy increased to varying degrees.

3.3.4. *In vitro* degradation. The degradation of polymer networks *in vitro* has been studied up to 24 week period. As shown in Fig. 6, all of polymer networks showed a higher degradation rate, where the weight of polymer networks decreased dramatically only after one week. Since PVP is not only a hydrophilic polymer, but a degradable polymer, introduced PVP in networks could quickly be degraded resulting in a significant mass loss of network. Moreover, during the first 8 weeks, all samples contained 2-PCL-F exhibited significant mass loss of more than 19% and a very similar degradation rate. In contrast, N-A50 had a mass loss of 14% within 8 weeks, which was smaller than that of samples with 2-PCL-F segment. The faster degradation could be attributed to the relative concentration of terminal hydroxyl group of the three samples as mentioned above caused by 2-PCL-F units.[27] When water molecules penetrated into the sample, the interaction between hydroxyl groups and water molecules accelerated the hydrolysis of polymer chain.

3.3.5. Biocompatibility of networks and anti-biofouling performance. To evaluate the biocompatibility of these networks, cell cytotoxicity experiments were performed. The extracts of specimen sheets were prepared for 1 day and 3 days, respectively, and used to cultivate MFCs. The compatibility and proliferation of MFCs were evaluated using CCK-8 assay.

MFCs were co-cultured with each sample extract for 24 h and 72 h, respectively. As shown in Fig. 7, the cell survival rates of all samples were higher than 90%, which indicated that the cytotoxicity of the samples was low. The growth and viability of cells were no significant difference among various extracts. Moreover, the number of cells cultured with sample extracts was gradually increasing as the time went by, as well as that on TCPS, indicating that there was no leached cytotoxic compound from the resultant networks. The morphology of MFCs cultured in the sample extracts for 1D, 3D and 5D was shown in Fig. 8. The MFCs adhered on each surface of PLLA/NVP network and PLLA/PCL/NVP network well, and showed a spread morphology as well as that on TCPS and HW-PLLA, indicating that no cytotoxicity could be found in the resultant networks.

To evaluate the cell adhesion and proliferation on the surface of resultant networks, MFCs were cultured on specimen sheets directly. Fig. 9 shows fluorescence microscopy images of DAPI and TRITC–phalloidin-stained MFCs growing on resultant networks and HW-PLA after 24 h and 72 h of
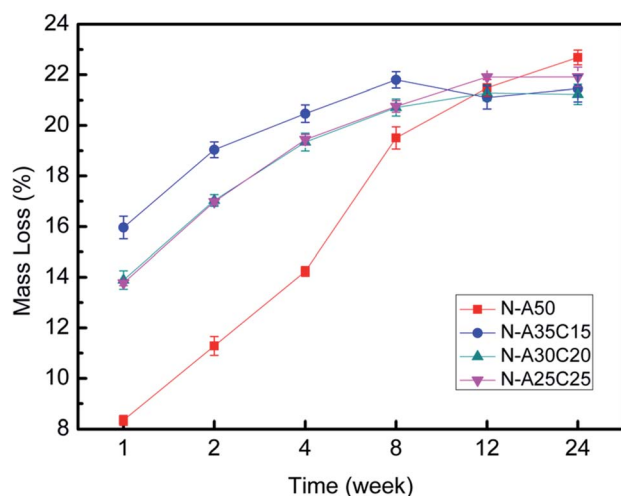

Fig. 6 The mass loss of N-A50, N-A35C15, N-A30C20, and N-A25C25 with the degradation over time.
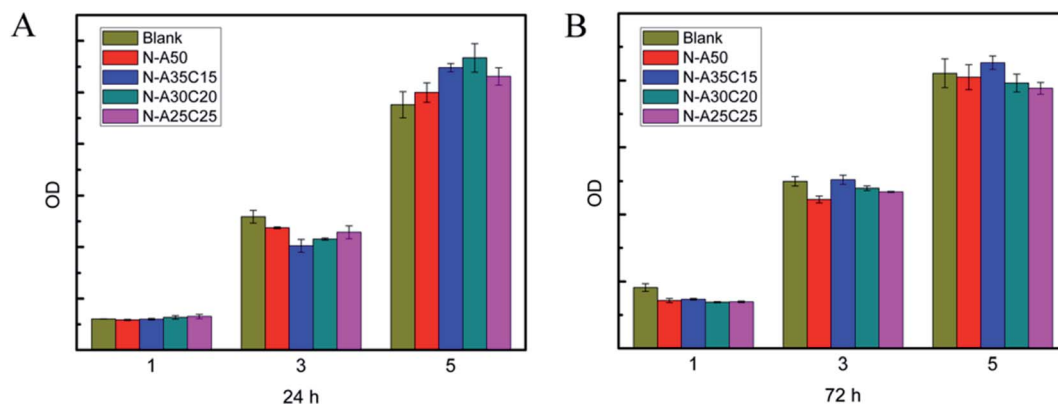
Fig. 7 Cell viability of fibroblast MFCs cultured in the samples' leaching liquor for 1, 3 and 5 days. The samples' leaching liquor has been prepared for 24 h (A) or 72 h (B).

incubation. After seeding on networks for 24 hours, MFCs barely adhered on the PLLA/PCL/NVP network and PLLA/NVP network. However, a few cells were observed on the surface of HW-PLA. After 72 h culture, the number of cells on the surface of HW-PLA increased significantly. In contrast, few cells were observed on the surface of N-A35C15, N-A30C20 and N-A25C25 polymer networks. The morphology of MFCs adhered on each surface has been visualized by SEM (Fig. 10). After 72 h incubation, MFCs were observed with a spindle shape on the surface of HW-PLA, which suggested that MFCs could adhere and spread on the surface of HW-PLA, and proliferate. Though a few of MFCs were found on the surface of N-A50 in Fig. 8, cells attached on the surface with a spherical shape by SEM study, which suggested a weak adhesion between cells and the

surface. Moreover, MFCs not only barely adhered on the surface of PLLA/PCL/NVP network, but presented a spherical shape. These results indicated that N-A35C15, N-A30C20 and N-A25C25 polymer networks had better anti-cell adhesion performance than that of N-A50.

Platelet-rich plasma contains clotting factors present in the plasma as well as proteins such as fibrinogen, contained within the α-granules of platelets, which are capable promoting clot formation. Adherence and activation of platelets are key steps of coagulation. Therefore, to evaluate the platelet adhesion and coagulation properties of the resultant specimens, *in vitro* experiments of platelet adsorption were used as assessment criteria. N-A35C15, N-A30C20, N-A25C25, N-A50 and HW-PLA samples were co-cultured with platelets for 1 h *in vitro* to
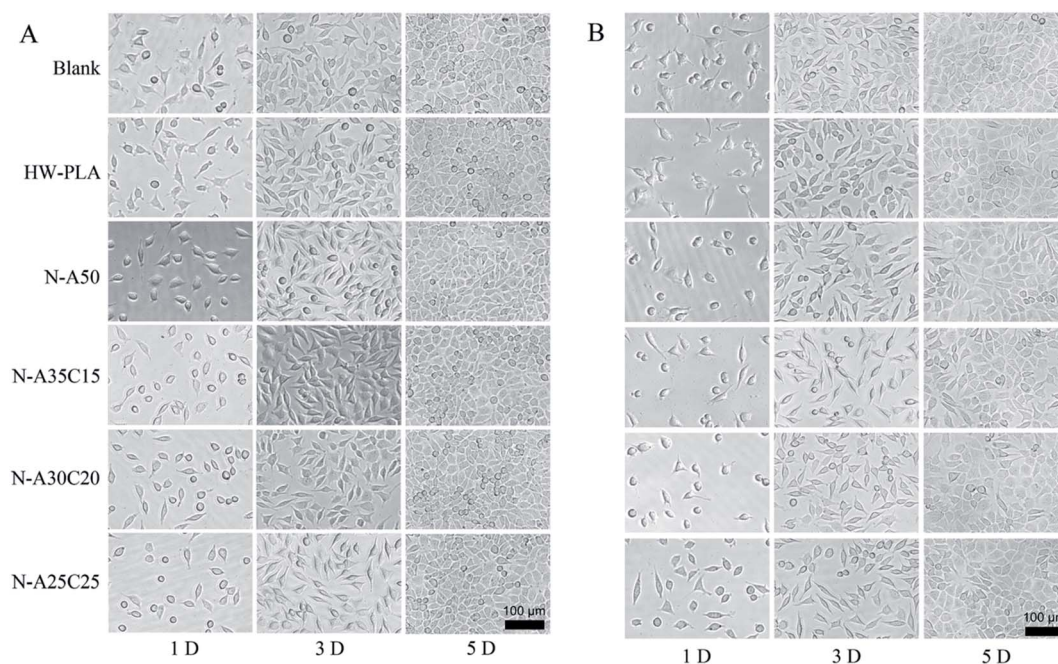

Fig. 8 The morphology of MFCs cultured in the samples' leaching liquor for 1, 3 and 5 days. The samples' leaching liquor has been prepared for 24 h (A) or 72 h (B).
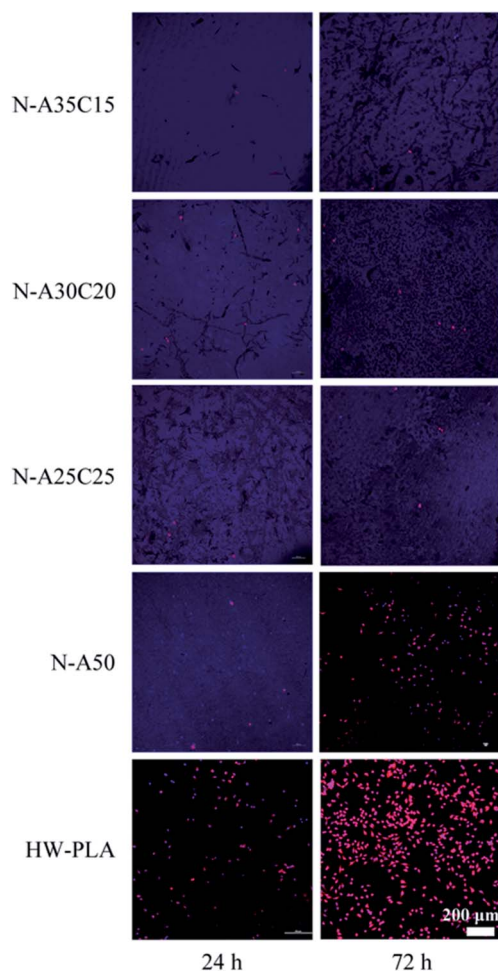
Fig. 9 Fluorescein stain images of MFCs seeding on polymer networks for 24 h or 72 h. The cells were labeled by DAPI and TRITC−phalloidin, and images were taken by a laser–scanning confocal microscope.

study the adhesion and activation of platelets. Hardly any platelets could be observed on the surface of N-A35C15, N-A30C20, N-A25C25 and N-A50 samples as visualized by SEM (Fig. 11). However, a significant number of platelets were adhered on HW-PLA surfaces. Moreover, the platelets on the surfaces of HW-PLA were observed in the severely activated and completely spread state. Obviously, the platelets produced pseudopods on smooth surfaces and tended to adhere to the surface. These results indicated that PLLA/PCL/NVP network could resist platelet absorption and activation as well as PLLA/NVP network.

The statistical results were given in Fig. 12A and B showed adhesion of *E. coli* to each sample after 4 h exposure to a bacterial suspension. The CFUs on LB agar plate of PLLA/NVP or PLLA/PCL/NVP networks were significantly lower than that of HW-PLA, indicating that PLLA/NVP or PLLA/PCL/NVP networks exhibited better anti-bacterial adhesion. Compared with N-A50, other specimens containing 2-PCL-F exhibited slightly fewer CFUs.

Based on the molecular level inside the cell, anti-cell adhesion is that the molecules on the surface of biomaterials could not be recognized with the receptor (protein) on the surface of cell membrane, so it cannot produce adhesion. Improving the hydrophilicity of surface could effectively resist the non-specific adsorption of proteins. Because the hydration layer would prevent direct contact between proteins and the surface, and strongly repel proteins close to the surface, which could avoid the protein adsorbing to the surface of material. PVP has been reported to form a stable and dense water barrier to avoid the adhesion of proteins and cells. Similarly, in this study, the hydrophilic segment of PVP content in N-A35C15, N-A30C20, and N-A25C25 as well as that in N-A50 could form a hydration layer on the surface of the material resulting in anti-biofouling surface. Moreover, the rest of hydroxyl groups surface in PLLA/PCL/NVP network could increase the hydrophily on the material as mentioned above, resulting in better anti-biofouling performance.
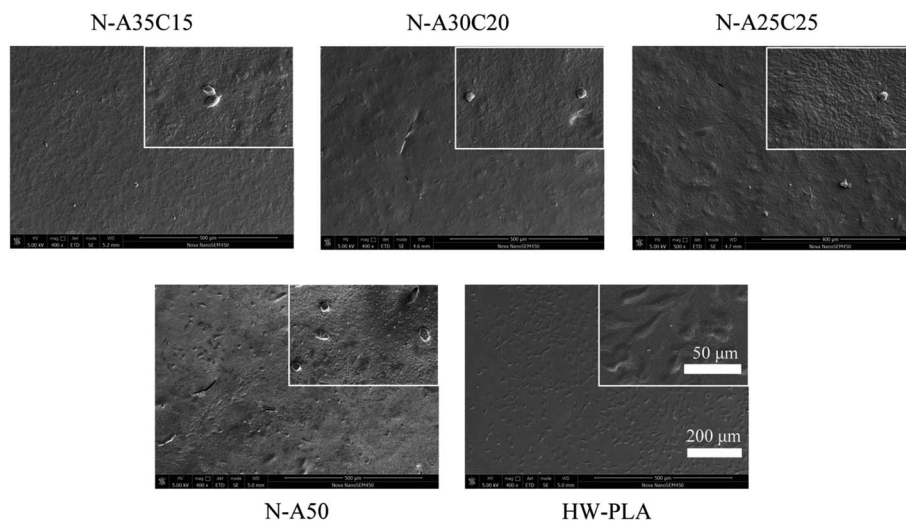

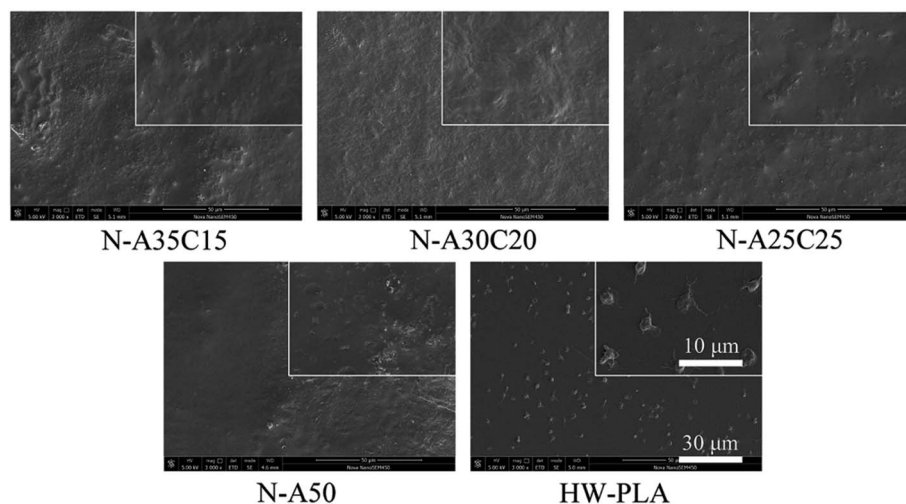**Fig. 10** SEM images of MFCs on polymer networks after 72 h.

Fig. 11 SEM images of platelets adhesion *in vitro*. SEM micrographs of samples after incubation in platelet-rich plasma.
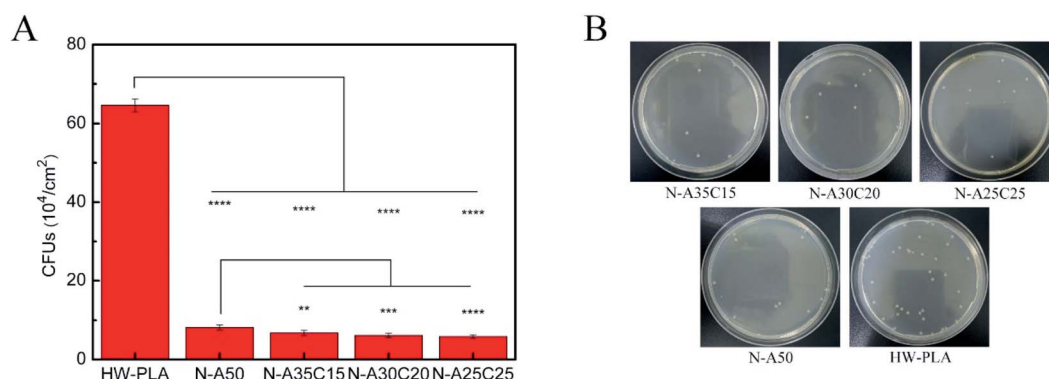

Fig. 12 The amount of CFUs that *E. coli* adheres to different networks was cultured for 1 d (A). Images of *E. coli* colonies on the HW–PLA, N–A50, N–A35C15, N–A30C20 and N–A25C25 surfaces after spread on agar plate (B). ns **$p < 0.01$, ***$p < 0.001$, ****$p < 0.0001$.

4. Conclusions

Photosensitive resin has been prepared by mixing 3-PLLA-F, 2-PCL-F, NVP as reactive diluent and Irgacure 2959 as photo-initiator, which could form PLLA/PCL/NVP cross-linked networks by UV irradiation. By increasing the segment of PCL content, the Young's modulus and tensile strength of resultant polymer networks decreased, but the elongation of networks increased significantly. No obvious cytotoxicity has been found in PLLA/PCL/NVP networks. Moreover, the PLLA/PCL/NVP networks could resist platelets and cells adhesion better than that of PLLA/NVP networks, because the rest of hydroxyl groups could enhance the hydrophilicity of material surface. Combined with UV-curing 3D Printing technology in the future, it is potential to develop an anti-biofouling material with the custom-fit requirements for medical applications.

Conflicts of interest

There are no conflicts to declare.

Acknowledgements

References

1 C. A. Del Grosso, C. Leng, K. Zhang, H.-C. Hung, S. Jiang, Z. Chen and J. J. Wilker, *Chem. Sci.*, 2020, **11**, 10367–10377.
2 J. Ma, C. Ma and G. Zhang, *Langmuir*, 2015, **31**, 6471–6478.
3 I. Dueramae, M. Nishida, T. Nakaji-Hirabayashi, K. Matsumura and H. Kitano, *J. Mater. Chem. B*, 2016, **4**, 5394–5404.
4 G. Dai, Q. Xie, C. Ma and G. Zhang, *ACS Appl. Mater. Interfaces*, 2019, **11**, 11947–11953.
5 R. van Lith, E. Baker, H. Ware, J. Yang, A. C. Farsheed, C. Sun and G. Ameer, *Adv. Mater. Technol.*, 2016, **1**, 1600138.
6 L. H. Sinh, K. Harri, L. Marjo, M. Minna, N. D. Luong, W. Jürgen, W. Torsten, S. Matthias and S. Jukka, *RSC Adv.*, 2016, **6**, 50706–50709.

7 Y. Wang, X. Lan, S. Zuo, Y. Zou, S. Li, Z. Tang and Y. Wang, *RSC Adv.*, 2021, **11**, 20997–21005.

8 L. G. Griffith, *Acta Mater.*, 2000, **48**, 263–277.

9 X. Chen, X. Wu, Z. Fan, Q. Zhao and Q. Liu, *Polym. Adv. Technol.*, 2018, **29**, 1684–1696.

10 K. Madhavan Nampoothiri, N. R. Nair and R. P. John, *Bioresour. Technol.*, 2010, **101**, 8493–8501.

11 T. Mao, G. Lu, C. Xu, H. Yu and J. Yu, *Prog. Org. Coat.*, 2020, **141**, 105317.

12 J. Jiang, L. Zhu, L. Zhu, H. Zhang, B. Zhu and Y. Xu, *ACS Appl. Mater. Interfaces*, 2013, **5**, 12895–12904.

13 Z. Wu, W. Tong, W. Jiang, X. Liu, Y. Wang and H. Chen, *Colloids Surf. B*, 2012, **96**, 37–43.

14 C. Zhang, T. Zhai, L.-S. Turng and Y. Dan, *Ind. Eng. Chem. Res.*, 2015, **54**, 9505–9511.

15 G. Maglio, A. Migliozzi, R. Palumbo, B. Immirzi and M. G. Volpe, *Macromol. Rapid Commun.*, 1999, **20**, 236–238.

16 L. Wang, W. Ma, R. A. Gross and S. P. McCarthy, *Polym. Degrad. Stab.*, 1998, **59**, 161–168.

17 C. Ma, W. Zhang, G. Zhang and P.-Y. Qian, *ACS Sustainable Chem. Eng.*, 2017, **5**, 6304–6309.

18 J. Yao, S. Chen, C. Ma and G. Zhang, *J Mater Chem B*, 2014, **2**, 5100–5106.

19 J. Jansen, M. P. Tibbe, G. Mihov, J. Feijen and D. W. Grijpma, *Acta Biomater.*, 2012, **8**, 3652–3659.

20 R. F. Storey, S. C. Warren, C. J. Allison and A. D. Puckett, *Polymer*, 1997, **38**, 6295–6301.

21 B. Sandner, S. Steurich and U. Gopp, *Polymer*, 1997, **38**, 2515–2522.

22 M. P. K. Turunen, H. Korhonen, J. Tuominen and J. V. Seppälä, *Polym. Int.*, 2001, **51**, 92–100.

23 J. F. Mano, Y. Wang, J. C. Viana, Z. Denchev and M. J. Oliveira, *Macromol. Mater. Eng.*, 2004, **289**, 910–915.

24 S. Jin, Y. Pu, Z. Guo, W. Zhu, S. Li, X. Zhou, W. Gao and B. He, *J Mater Chem B*, 2021, **9**, 3863–3873.

25 J. Teng, S. Bates, D. A. Engers, K. Leach, P. Schields and Y. Yang, *J. Pharm. Sci.*, 2010, **99**, 3815–3825.

26 T.-T. Li, H. Zhang, S.-Y. Huang, X. Pei, Q. Lin, S. Tian, Z. Ma and J.-H. Lin, *J. Polym. Res.*, 2021, **28**, 156.

27 H. Tsuji and Y. Ikada, *J. Appl. Polym. Sci.*, 1998, **67**, 405–415.